Results in Control and Optimization 25 (2026) 100871

Contents lists available at ScienceDirect

Results in Control and Optimization

journal homepage: www.elsevier.com/locate/rico

Efficient quality control of Maxwell-distributed processes: A new control charting strategy with industrial application

Zahid Khan [a], Attila I. Katona [b,a], Zsolt T. Kosztyán [b,a,c,*]

[a] Business Research Institute for Data-Driven Growth and Economics (BRIDGE), Faculty of Business and Economics University of Pannonia, Veszprém, Hungary

[b] Department of Quantitative Methods, Institute of Management, Faculty of Business and Economics, University of Pannonia, Veszprém, Hungary

[c] Institute of Advanced Studies, Kőszeg (iASK), Kőszeg, Hungary

ARTICLE INFO

Keywords:
Memory type chart
Maxwell process
Estimation
Homogeneous weights
V chart
VEWMA chart

ABSTRACT

The Maxwell distribution is important in engineering applications when analyzing stochastic phenomena. In recent years, control charts based on the Maxwell process have attracted attention due to the limitations of traditional control chart schemes, which typically assume normality, a condition that is often violated in real-world engineering applications. This issue is particularly evident in scenarios in which the Maxwell process better represents the underlying data generation process, making Maxwell-based V and VEWMA control charts more suitable for improving and efficiently monitoring such processes. One significant advancement in process monitoring is the increasing popularity of the homogeneously weighted moving average (HWMA) control chart and its various extensions, which introduce a new approach to memory-type control charts. In this study, we introduce a new control chart, called the Maxwell homogeneously weighted moving average (MHWMA), for monitoring the scale parameter of the underlying Maxwell quality characteristic. The proposed scheme assigns the greatest weight to the most recent sample, while the remaining weight is distributed evenly across all previous samples. The parameters of the proposed chart are derived, and its effectiveness is evaluated by using run length (RL) distribution metrics. To evaluate the effectiveness of the MHWMA chart, it is compared with other competing charts from the same family that are typically utilized for Maxwell-distributed data. The numerical results indicate the superiority of the proposed chart over the existing control charts. Finally, a real data example is analyzed to complement and validate the theoretical findings of the work.

1. Introduction

In statistical process control (SPC), statistical approaches are applied for effective monitoring and control of manufacturing processes [1]. With SPC, industries aim to keep processes stable, pinpoint specific issues and enable timely corrective actions through a robust control system [2]. Regardless of whether a product or a service is physically good, quality management integrates various SPC and management techniques to produce products of excellent quality [3]. Ultimately, client satisfaction with products or services is the primary concern of most organizations [4]. A company will face significant difficulty selling its products or services if clients are not satisfied with a product's quality [5]. The control chart thus stands out as a crucial approach within the SPC toolkit for effectively accomplishing these objectives [6]. Consequently, control charts have been broadly applied in the manufacturing and

* Corresponding author.
E-mail addresses: katona.attila@gtk.uni-pannon.hu (A.I. Katona), kosztyan.zsolt@gtk.uni-pannon.hu (Z.T. Kosztyán).

https://doi.org/10.1016/j.rico.2026.100871
Received 9 July 2026; Received in revised form 26 September 2026; Accepted 26 October 2026
Available online 4 November 2026
2666-7207/© 2026 The Authors. Published by Elsevier B.V. This is an open access article under the CC BY license (http://creativecommons.org/licenses/by/4.0/).

service sectors and are used to facilitate the monitoring and control of production processes. By monitoring and identifying irregular variations, control charts refine product quality and increase process productivity [7]. In other words, they facilitate optimized productivity and output regulation. The field of SPC spans numerous types of control charts [8]. Notably, Shewhart charts are specifically designed to detect substantial shifts in process behavior [9]. Another popular category comprises memory-type charts such as exponentially weighted moving average (EWMA) and cumulative sum (CUSUM) charts, which are favored in the process and service industries for promptly identifying quick responsiveness to small-to-moderate changes in monitoring parameters [10,11]. The sensitivity of CUSUM and EWMA charts to minor shifts in process parameters is enhanced due to the utilization of both current and historical process data [12].

To optimize performance by integrating the advantages and addressing the drawbacks of memory-less and memory-type control charts, various extensions have been developed, as noted in the SPC literature. The use of mixed control charts has been suggested to increase detection capability. The designs for combined Shewhart-EWMA charts and Shewhart-CUSUM charts were suggested by Lucas [13] and Lucas and Saccucci [14], respectively. Studies have revealed that the Shewhart-EWMA chart is a more sensitive detection tool than the standalone EWMA chart and have cautioned against the use of the Shewhart-EWMA chart in processes that are prone to occasional outliers. Zaman et al. [15] introduced a mixed CUSUM-EWMA (MCE) charts, while Abbas et al. [16] proposed a mixed EWMA-CUSUM (MEC) control charts for more comprehensive and balanced detection capability for a wider range of process changes. Sheu and Lin [17] advanced control charting by introducing generally weighted moving average (GWMA) charts and they also proposed a combined Shewhart-GWMA charts to enhance the detection ability of the GWMA chart for substantial shifts. Ali and Haq [18] contributed the mixed GWMA-CUSUM control chart to monitor the process mean. Similarly, expanding on existing methods, Taboran et al. [19] developed mixed moving average- exponentially weighted moving average (MA-EWMA) charts, and Talordphop et al. [20] proposed the modified exponentially weighted moving average-moving average (MEWMA-MA) control chart for systems that follow standard or nonstandard distributions. By utilizing the idea of the HWMA control chart proposed by Abbas [21], Abid et al. [22], Abid et al. [23] established the combined HWMA with CUSUM (HWMA-CUSUM) control charts which are more effective than typical control charts. To concurrently investigate changes in both the mean and dispersion of the process, Zaman et al. [24] designed a set of mixed control charts. Inspired by the work of Lucas [13], ur Rehman et al. [25] suggested the Shewhart-Crosier CUSUM (CCUSUM) chart, which is marginally more effective for small changes than the Shewhart-CUSUM chart. More recently, Talordphop et al. [26] introduced a moving average (MA) with an HWMA chart (MA-HWMA) for monitoring the process mean. Beyond time-weighted and mixed schemes, recent research has also advanced control chart design through enhanced sampling structures and more informative run length metrics. In particular, double sampling and synthetic double sampling charts have been developed and evaluated using the median run length (MRL) and expected median run length (EMRL), which are more appropriate than the average run length (ARL) when the RL distribution is highly skewed [27–30]. These developments highlight the need for enhanced control strategies and robust performance measures when monitoring non-normal or skewed processes.

Control charts are typically employed in monitoring processes under the assumption that the measured quality characteristics exhibit a normal distribution. However, in practice, many real-world quality characteristics follow asymmetrical models; in these situations, the application of process charts that presume normality can lead to inaccurate conclusions about a process's actual state. There has been a growing trend in recent EWMA design work to consider underlying nonnormal processes, and this focus has led to extensive research over the past few years into both the standard and advanced EWMA control chart designs as targeted processes specifically for nonnormal data generation. This field has been supported by substantial input from studies by Borror et al. [31], Noiplab and Mayureesawan [32], Noorossana et al. [33], Huwang and Lin [34], Alduais and Khan [35], Sanaullah et al. [36]. The robustness of EWMA control charts against heavy-tailed and skewed distributions was also examined by Human et al. [37]. Liu et al. [38] focused on the transformed exponential and Weibull distributions to develop robust EWMAs, and Abbasi et al. [39] introduced new EWMA charts based on various dispersion estimators for both normal and nonnormal distributions. Saghir et al. [40] developed a modified EWMA control chart by using a transformation approach to monitor gamma-distributed processes. Gan [41] outlined a method to develop an EWMA specifically for binomial observations, and while considering a negative binomial distribution as an appropriate model, Urbieta et al. [42] described an EWMA control chart for daily hospitalizations. Ryan and Woodall [43] suggested an EWMA design for monitoring Poisson count data. Furthermore, EWMA designs based on the weighted and reflected power function distributions have been developed for monitoring reliability processes [44,45]. For more information on enhanced EWMA designs applied to nonnormal processes, see the works by Calzada and Scariano [46], Alkahtani [47], Lin et al. [48], Saeed and Kamal [49], Saeed and Abu-Shawiesh [50], Nazir et al. [51], Sanaullah et al. [36]. Since many real-world quality characteristics deviate from normality, there remains a persistent gap in terms of effective control charts designed specifically for asymmetric data, emphasizing the ongoing demand for advanced monitoring schemes that do not rely on the traditional assumption of normality.

The Maxwell distribution, known for its positively skewed shape, is well suited for modeling various real-world phenomena, particularly in engineering applications that involve particle speeds, reliability analysis, and lifetime data [52–57]. To address situations in which the data are not normally distributed, several researchers have introduced control charts for Maxwell family processes. For instance, Godase et al. [58] proposed one- and two-sided sequential probability ratio test (SPRT) control charts to monitor the scale parameter of a Maxwell distribution process, which demonstrated superior performance over traditional Shewhart charts. Shah et al. [59] introduced a control chart for the scale parameter of the Maxwell distribution under the assumption that the underlying data are imprecise and contain vague information, and Arafat et al. [60] developed the EWMA chart, namely, the inverse Maxwell EWMA (IMEWMA) chart, which is specifically designed for processes that fit an inverse Maxwell distribution. Saghir et al. [61] devised another optimized scheme to monitor inverse Maxwell quality characteristics by using a Markov chain model. Another extended adaptive EWMA control chart for monitoring processes that follow an inverse Maxwell distribution was suggested

by Waqas et al. [62]. Shah et al. [63] developed the VSQ-chart as a graphical tool to monitor the parameters of Maxwell processes, and time-weighted control chart variants of the VSQ-charts have been proposed in previous studies [10,11]. Considering the squared scale parameter as a key characteristic of the Maxwell distribution, Hossain et al. [64] developed a V-chart for monitoring Maxwell-distributed data. Furthermore, enhancements for detecting smaller changes in this parameter have been explored in previous studies by using EWMA and CUSUM approaches [65,66].

In recent years, the HWMA approach has been increasingly adopted in quality control research [67,68]. By using an optimized weighting scheme, Abbas [21] originally introduced an HWMA chart designed to efficiently detect small to moderate process shifts. Due to the effectiveness of the HWMA over the EWMA, the structure of the HWMA has been adopted in numerous other studies [22,57,67,69–74].

All of the aforementioned studies provide strong evidence for exploring and developing the suitability of the HWMA-based control chart for processes that follow the Maxwell distribution. Real-world data often deviate from normality, necessitating efficient control chart designs that accommodate nonnormal behaviors. To the best of our knowledge, no prior research has explored the application of the HWMA structure to nonnormal distributions such as the Maxwell distribution. Motivated by this gap, this study introduces an HWMA control chart specifically for monitoring the scale parameter of the Maxwell distribution. To date, no HWMA-based control chart that is explicitly designed for the Maxwell process has been reported in the literature. Consequently, this work makes the following three significant contributions to the field:

[C1] This work develops a novel homogeneous weighting scheme-based control chart uniquely adapted to the Maxwell distribution, filling a critical gap in the current research.

[C2] The proposed method establishes the HWMA framework as a superior alternative to conventional methods, offering more efficient and timely detection of process changes.

[C3] This study validates the applicability and effectiveness of the proposed MHWMA scheme in real-world scenarios, highlighting its potential for practical deployment in quality control systems.

In contrast to the traditional EWMA scheme designed for Maxwell distributed processes, the proposed MHWMA chart employs a homogeneous weighting structure that effectively improves the detection of shifts in Maxwell-distributed characteristics (see [C1]). By optimally balancing the influence of recent and historical observations, the proposed chart provides quicker and more accurate detection of process changes. Analytical developments and Monte Carlo results reveal the superior sensitivity of the proposed model compared with its existing counterparts (see [C2]). Additionally, the successful implementation of the MHWMA chart on aerospace industry data demonstrates the applicability of the proposed method to real-world Maxwell-type processes (see [C3]). Collectively, these findings strengthen the utility of the proposed framework for modern quality control applications in which Maxwell-type variations are encountered.

This paper is organized as follows: Section 2 describes the preliminary results related to the Maxwell distribution and some of its key properties. Details regarding the proposed chart are provided in Section 3, and Section 4 covers the assessment and evaluation of the proposed MHWMA control chart in terms of the run RL distribution. A comparative study of the proposed chart with other memory-type control charts of the same class is presented in Section 5. The steady-state performance analysis is presented in Section 6. A real data example is then presented in Section 7 to illustrate how the MHWMA chart can be implemented in practical scenarios. The article concludes by summarizing the main findings in Section 8.

2. Preliminary results

In this section, the Maxwell distribution (MD) and key features relevant to control chart development are explored. Our analysis proceeds with the assumption that the underlying quality characteristic is modeled by a single-parameter MD. Assuming that the quality characteristic Y follows the Maxwell model with scale parameter β, it can be characterized by using its probability density function (PDF) and cumulative distribution function (CDF), which are defined as follows:

$$G(y,\beta) = \frac{2}{\sqrt{\pi}}\gamma\left(\frac{3}{2},\frac{y^2}{2\beta^2}\right), \quad \beta>0,\ y>0, \tag{1}$$

$$g(y,\beta) = \sqrt{\frac{2}{\pi}}\cdot\frac{y^2}{\beta^3}\exp\left(-\frac{y^2}{2\beta^2}\right), \quad \beta>0,\ y>0. \tag{2}$$

These functions are parameterized by β, which controls the scale (spread) of the distribution. Characterized by its positively skewed structure, the MD is commonly used in fields such as physics, analytical chemistry and reliability engineering.

In practical applications, the parameter β is typically unknown and is thus estimated with the methods outlined by Krishna et al. [55]. A review of the literature reveals that maximum likelihood estimation (MLE) is the most often used method for estimating the parameter β. Based on standard MLE approach, the following estimator is used to estimate the parameter β [64]:

$$\hat{\beta} = \sqrt{\frac{\sum_{i=1}^{n} {y_{ik}}^2}{3n}} \tag{3}$$

The sampling distribution of $\hat{\beta}$ is not well known; therefore, the following estimator T is used to identify changes in the Maxwell distributed quality characteristics:

$$T_k = \frac{\sum_{i=1}^{n} {y_{ik}}^2}{3n} \tag{4}$$

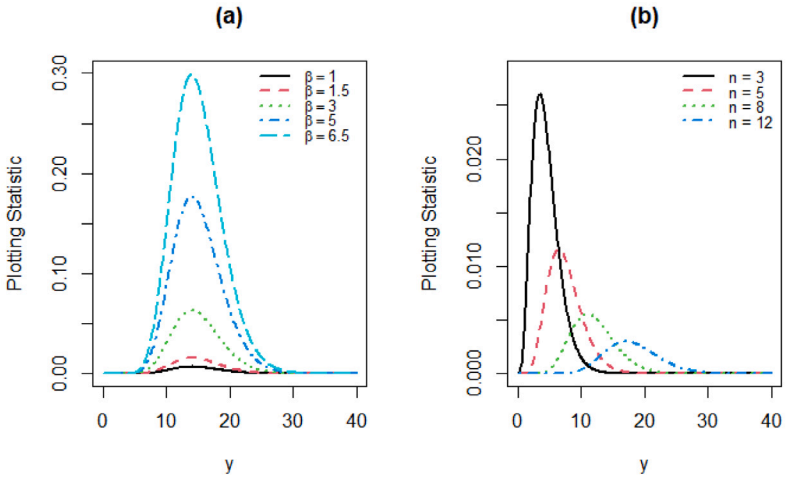


Fig. 1. Density plot of the T_k estimator at fixed (a) $n = 10$ (b)$\beta = 1.5$

Consider $y_{1k}, \ldots, y_{nk}$ to be the kth sample of size n drawn from the Maxwell model, i.e., $Y_{i,k} \sim \text{MD}(\beta)$ for $i = 1, 2, \ldots, n$. β represents the scale parameter of the Maxwell distributed quality characteristic. Let T_k denotes the sample estimator of β^2, which is estimated by using Eq. (4) for the kth subgroup. By employing Eq. (2), it can be easily proven that if Y follows MD(β), then the random variable $Y^2/2\beta^2$ follows Gamma(3/2, 1), and by using the additive property of independent identical Gamma random variables, the random variable $Z = \sum Y_i^2/2\beta^2$ follows Gamma (3n/2, 1). Thus, the plotting statistic $T = \frac{2\beta^2}{3n} Z$ follows $Gamma\left(\frac{3n}{2}, \frac{2\beta^2}{3n}\right)$, based on the property that if $Y \sim Gamma(\alpha, \beta)$, then $cY \sim Gamma(\alpha, c\beta)$. The two side-by-side subplots of the plot statistic T_k under different values of the scale parameter β and sample size n are shown in Fig. 1.

As shown in Fig. 1, noticeable skewness persists unless there is a substantial increase in the sample size and/or the scale parameter β. Fig. 1(a) examines how the scale parameter β affects the density plot when the sample size is fixed. A higher value of β stretches the density upward and shifts the mass slightly to the right, which means that the spread of the distribution becomes wider with higher β as it controls the scale of the data. On the other hand, Fig. 1(b) indicates the influence of the sample size on the shape of the sampling distribution, which keeps the scale fixed. A higher value of n causes the Gamma distribution to be more concentrated toward the center and leads to symmetry, which supports the consistency property of the MLE estimator. These findings indicate that sample size is a crucial factor that affects control chart reliability and sensitivity. Because of the practical limitations mentioned in the literature [75], the selection of a moderate or small value for n, which is typically in the range of 1 to 10, is necessary. Now, the mean and variance of the estimator T_k can be easily obtained and used to establish control limits for the Shewhart type V control chart model and are expressed as follows:

$$\begin{aligned} \text{LCL} &= W_1\beta^2 = \left[1 - L\sqrt{\frac{2}{3n}}\right]\beta^2 \\ \text{UCL} &= W_2\beta^2 = \left[1 + L\sqrt{\frac{2}{3n}}\right]\beta^2 \end{aligned} \tag{5}$$

where the values of the constants W_1 and W_2 can be found in Hossain et al. [64]. The control limit coefficient L is determined from the quantile of the Gamma distribution so that the desired false alarm rate α is achieved.

If the underlying process data are nonnormal and particularly skewed, such as in the Maxwell distribution, the limits established by Eq. (5) might not correspond to the intended false alarm rate. Consequently, this phenomenon leads to too many missed detections due to wider control limits or too many false alarms due to narrow control limits. Alternatively, probability limits are used since they are based on the actual percentiles from the real distribution of the statistics. The probability limits of the V chart are defined as [64]:

$$\begin{aligned} \text{LPL} &= \frac{2\beta^2}{3n}\,\boldsymbol{\Phi}^{-1}\left(\frac{\alpha}{2}\right) \\ \text{UPL} &= \frac{2\beta^2}{3n}\,\boldsymbol{\Phi}^{-1}\left(1 - \frac{\alpha}{2}\right) \end{aligned} \tag{6}$$

where α is the false alarm rate (Type-I error probability) and $\boldsymbol{\Phi}^{-1}(\cdot)$ is the Gamma distribution quantile evaluated at $\alpha/2$ and $1-\alpha/2$ for the lower and upper limits, respectively. Eq. (5) follows the general structure of the Shewhart-type model, which is designed for processes in which large deviations need immediate attention. This approach treats each data point (or subgroup) independently and uses current measurements to assess the process stability. Time-weighted control charts, such as EWMA chart, use weighted historical data to detect subtle changes or drifts in the Maxwell process over time and were presented in Hossain and Riaz [66].

The proposed approach for the EWMA chart, known as the VEWMA chart, is suitable for Maxwell processes in which small shifts are critical. By utilizing the EWMA charting structure, the plotting statistic for the VEWMA scheme can be expressed as follows:

$$W_i = \theta T_i + (1-\theta)W_{i-1} \tag{7}$$

where W_i denotes the current value of the plotting statistic, T_i is the current value of the MLE given in Eq. (4), and the smoothing constant θ $(0 < \theta \leq 1)$ determines the relative weight pattern given to the most recent observation. Alternatively, Eq. (7) can be expressed as follows:

$$W_j = \sum_{i=0}^{j-1} \theta(1-\theta)^i T_{j-i} + (1-\theta)^j W_0 \tag{8}$$

Eq. (8) presents the EWMA in different ways, where the term $(1-\theta)^j W_0$ incorporates the influence of the initial value and the weights $\theta(1-\theta)^i$ decay geometrically by a factor of $(1-\theta)$ for each step back in time. Analogous to the EWMA scheme, the initial value W_0 is set to the monitoring parameter β^2. If the target scale parameter is unknown, it can be estimated on the basis of the average of the preliminary dataset. Since the statistic T follows a gamma distribution with parameters $\frac{3n}{2}$ and $\frac{2\beta^2}{3n}$, the control limits of the VEWMA charting scheme can be expressed as follows:

$$\text{LCL} = Q_1\beta^2, \quad \text{CL} = \beta^2, \quad \text{UCL} = Q_2\beta^2 \tag{9}$$

where the constants $Q_1 = \left[1 - k\sqrt{\frac{2\theta}{3n(2-\theta)}\left(1-(1-\theta)^{2i}\right)}\right]$ and

$Q_2 = \left[1 + k\sqrt{\frac{2\theta}{3n(2-\theta)}\left(1-(1-\theta)^{2i}\right)}\right]$ with a gamma quantile point k can easily be obtained for various values of the smoothing constant θ, sample size (n) and false alarm rate α, as described by Hossain and Riaz [66]. While the VEWMA charting scheme demonstrates a strong ability to promptly detect small disturbances in the Maxwell process, its performance may be suboptimal under certain practical conditions. To further enhance its performance, the subsequent section proposes an HWMA-type charting approach with a modified weighting scheme.

3. Proposed control chart

Assume that the quality characteristic to be monitored, denoted by Y_{ik}, follows a one-parameter $MD(\beta)$, where $i = 1, 2, 3, \ldots, n$ and $k = 1, 2, 3, \ldots, M$. Initially, it is assumed that the population parameter β is known, i.e., $\beta = \beta_0$. The plotting statistic of the proposed MHWMA chart is defined as follows:

$$P_k = \rho H_k + (1-\rho)Q_{k-1} \tag{10}$$

where $Q_{k-1} = \frac{\sum_{i=1}^{k-1} T_i}{k-1}$ is the mean of the previous $(i-1)$ sample values and the initial value Q_0 is set equal to monitoring β^2. The parameter ρ is known as a sensitivity parameter of the MHWMA control chart and H_k is the plotting statistic of the HWMA.

The structure of H_k in terms of the Maxwell MLE estimator (T_k) is defined as follows:

$$H_k = \rho T_k + (1-\rho)Q_{k-1} \tag{11}$$

Substituting Eq. (11) in Eq. (10) yields:

$$P_k = \rho^2 T_k + (1-\rho^2)Q_{k-1} \tag{12}$$

Eq. (12) clearly indicates that the current sample receives a weight of ρ^2 while the remaining weight $(1-\rho^2)$ is distributed uniformly across all past samples. From Eq. (12), the mean and variance of the plotting statistic can be derived as follows:

For $k = 1$

$$E(P_1) = \rho^2 E(T_1) + (1-\rho^2)Q_0 = \beta^2 \tag{13}$$

Since $T_1, T_2 \ldots T_M$ are independent Gamma random variables with mean $E(T_i) = \beta^2$ and variance $V(T_i) = \frac{2\beta^4}{3n}$, then:

$$E(P_1) = \rho^2\beta^2 + (1-\rho^2)\beta^2 = \beta^2 \tag{14}$$

$$Var(P_1) = \rho^4 Var(T_1) = \frac{2\rho^4\beta^4}{3n} \tag{15}$$

For $k > 1$

$$E(P_k) = \rho^2 E(T_k) + (1-\rho^2)E(Q_{k-1}) \tag{16}$$

Before proceeding further, we must first find the mean and variance of the Q_{k-1} statistic. The mean of the Q_{k-1} statistic is expressed as follows:

$$E\left(Q_{k-1}\right) = \frac{\sum_{i=1}^{k-1} E\left(T_i\right)}{k-1} \tag{17}$$

After simplification, Eq. (17) becomes:

$$E\left(Q_{k-1}\right) = \beta^2 \tag{18}$$

Similarly, the variance of the Q_{k-1} statistic is defined by:

$$Var\left(Q_{k-1}\right) = \frac{\sum_{i=1}^{k-1} Var\left(T_i\right)}{(k-1)^2} \tag{19}$$

By simplifying Eq. (19), we obtain the following:

$$Var\left(Q_{k-1}\right) = \frac{2\beta^2}{3n(k-1)} \tag{20}$$

By substituting Eq. (18) into Eq. (16) yielded:

$$E(P_k) = \rho^2\beta^2 + (1-\rho^2)\beta^2 = \beta^2 \tag{21}$$

Now, the variance of the plotting statistic can be derived easily as follows:

$$Var(P_k) = \rho^4 Var(T_k) + (1-\rho^2)^2 Var(Q_{k-1}) + 2\rho^2(1-\rho^2)Cov(T_k, Q_{k-1}) \tag{22}$$

where $Cov(T_k, Q_{k-1})$=0 represents the $T_1, T_2, \ldots, T_{k-1}$ values of the Maxwell statistics computed independently from all of the subgroups.

Thus, substituting Eq. (20) in Eq. (22) and simplifying yields the following:

$$Var(P_k) = \frac{2\rho^4\beta^4}{3n} + \frac{2(1-\rho^2)^2\beta^2}{3n(k-1)} \tag{23}$$

Thus, the control limits of the proposed charts can be established as follows:

$$\begin{aligned}
LCL &= \begin{cases} \beta^2 - L\beta^2\sqrt{\frac{2}{3n}\rho^4}, & k = 1, \\ \beta^2 - L\beta^2\sqrt{\frac{2}{3n}\left(\rho^4 + \frac{(1-\rho)^2(1+\rho)^2}{k-1}\right)}, & k > 1, \end{cases} \\
CL &= \beta^2, \\
UCL &= \begin{cases} \beta^2 + L\beta^2\sqrt{\frac{2}{3n}\rho^4}, & k = 1, \\ \beta^2 + L\beta^2\sqrt{\frac{2}{3n}\left(\rho^4 + \frac{(1-\rho)^2(1+\rho)^2}{k-1}\right)}, & k > 1. \end{cases}
\end{aligned} \tag{24}$$

where the factor L controls the width of the control limits and can be determined based on the desired in-control ARL (ARL_0) value using a simulation approach.

Eq. (24) can be equivalently written as follows:

$$\begin{aligned}
LCL &= \beta^2 M_1, \\
CL &= \beta^2, \\
UCL &= \beta^2 M_2.
\end{aligned} \tag{25}$$

where $M_1 = 1 - L\sqrt{\frac{2}{3n}\left(\rho^4 + \frac{(1-\rho^2)^2}{k-1}\mathbf{I}_{\{k>1\}}\right)}$ and $M_2 = 1 + L\sqrt{\frac{2}{3n}\left(\rho^4 + \frac{(1-\rho^2)^2}{k-1}\mathbf{I}_{\{k>1\}}\right)}$ are two constant values with indicator function I, which is defined as follows:

$$\mathbf{I} = \begin{cases} 1, & \text{if } k > 1, \\ 0, & \text{if } k = 1. \end{cases}$$

It can easily be seen that the coefficients M_1 and M_2 approach stable values as $k \to \infty$, the fraction $\frac{(1-\rho^2)^2}{k-1} \to 0$. To construct the proposed chart, it is highly recommended that the chart be constructed with the precise parameters provided in Eq. (25). When the value of the plotting statistic P_k is outside the LCL and UCL control limits, the process is assumed to be unstable. Consequently, corrective actions should be taken to quickly identify and resolve any special causes of variation. It is worth noting that, since the coefficients M_1 and M_2 do not depend on β, the control limits scale proportionally with β^2 as the process dispersion increases, thereby preserving the relative width of the control region regardless of the magnitude of β. However, when β is large and M_1 is negative (as can occur for small k), the resulting LCL becomes negative; since the plotting statistic P_k is non-negative by construction, such limits are truncated at zero, i.e., LCL = $\max(\beta^2 M_1, 0)$.

When the value of the monitoring parameter is known, the aforementioned application of the proposed chart is feasible. In many instances, process parameters are often unavailable, leading to the use of a retrospective approach in which historical data from periods when the process was assumed to be IC can be used to determine their values.

Table 1
Control limit coefficients of the MHWMA chart at $ARL_0 = 370$.

Sample size	$\rho = 0.03$	$\rho = 0.05$	$\rho = 0.10$	$\rho = 0.25$	$\rho = 0.50$	$\rho = 0.75$
2	1.805592	1.622772	1.633453	2.846527	3.898239	4.034805
3	1.831949	1.615524	1.632977	2.753830	3.704643	3.820038
4	1.760185	1.635075	1.622438	2.688885	3.550828	3.672361
5	1.821041	1.672268	1.630783	2.667427	3.463268	3.587723
6	1.811922	1.671284	1.635700	2.652347	3.391653	3.511190
7	1.836151	1.656532	1.621395	2.642512	3.34668	3.463626
8	1.800537	1.670778	1.623809	2.632380	3.301024	3.403783
9	1.819611	1.662344	1.630604	2.625793	3.261924	3.366351
10	1.810610	1.678646	1.624107	2.624512	3.248870	3.348529

Table 2
Components M_1 and M_2 for the MHWMA chart at $\rho = 0.03$.

Time index (k)	Sample size = 4		Sample size = 6		Sample size = 8	
	M_1	M_2	M_1	M_2	M_1	M_2
1	0.9994	1.0006	0.9995	1.0005	0.9995	1.0005
2	0.2821	1.7179	0.3966	1.6034	0.4807	1.5193
3	0.4923	1.5077	0.5733	1.4267	0.6328	1.3672
4	0.5855	1.4145	0.6516	1.3484	0.7002	1.2998
5	0.6410	1.3590	0.6983	1.3017	0.7403	1.2597
6	0.6789	1.3211	0.7301	1.2699	0.7678	1.2322
7	0.7069	1.2931	0.7536	1.2464	0.7880	1.2120
8	0.7286	1.2714	0.7719	1.2281	0.8037	1.1963
9	0.7462	1.2538	0.7867	1.2133	0.8164	1.1836
10	0.7607	1.2393	0.7989	1.2011	0.8269	1.1731
11	0.7730	1.2270	0.8092	1.1908	0.8358	1.1642
12	0.7835	1.2165	0.8181	1.1819	0.8434	1.1566

In the case of an unknown value of β, Eq. (25) can be written as follows:

$$\begin{aligned} LCL &= \hat{\beta}^2 M_1, \\ CL &= \hat{\beta}^2, \\ UCL &= \hat{\beta}^2 M_2. \end{aligned} \tag{26}$$

where $\hat{\beta}^2 = \frac{\sum_{k=1}^{M} T_k}{M}$ represents the overall mean value of the estimated values of T_k obtained from M subgroups collected over time. In practice, the quality characteristic is controlled by using a two-phase procedure. In Phase I, a set of M preliminary subgroups collected under presumed in-control conditions is used to compute $\hat{\beta}^2$, which is then substituted into Eq. (26) to obtain the estimated control limits. In Phase II, these estimated limits are used to monitor future subgroups: for each new subgroup, the plotting statistic P_k is computed via Eq. (12) and compared with the estimated LCL and UCL. The process is declared out-of-control (OC) if P_k falls outside these limits. This procedure is illustrated in Section 7 using the real windshield failure dataset.

The choice of control limits plays a vital role in the design of control charts. In this study, the limits are determined such that an ARL_0 equal to approximately 370 is achieved, and we utilize a simulation approach to find the charting constant L (see Appendix). Table 1 provides the values of L for different combinations of n and ρ at a fixed value of ARL_0.

The results in Table 1 illustrate how the values of the control limit coefficient L vary with changes in both the sample size and smoothing constant values. The control limit coefficient values are particularly important because they determine the chart's ability to detect process changes. In other words, these values determine the sensitivity of the chart, balancing the risk of false alarms against the detection speed. This information offers practical guidance for setting appropriate control limits for specific performance needs. Additionally, Tables 2 and 3 provide the values of the components M_1 and M_2, which can be used to determine the control limits of the proposed chart without computing the control limit coefficient L.

Tables 2 and 3 provide the coefficients M_1 and M_2, which can be used to estimate the width of the MHWMA control chart. The results in Tables 2 and 3 also show how sample size (n), smoothing constant (ρ) and time index (k) influence the values of these coefficients. The coefficients M_1 and M_2 clearly exhibit a time-varying pattern. The results indicate a steady increase in the values of M_1 and M_2 and a steady decreases toward stable values as $k \geq 2$. At the initial time point (k=1), both coefficients are near 1, yielding nearly symmetric control limits. The results also indicate that increasing the sample size consistently reduces the spread between M_1 and M_2, yielding tighter control limits and higher sensitivity. Moreover, the value of LCL can be negative due to the mathematical structure of M_1. This situation arises legitimately from the mathematical structure of the M_1 coefficient, but it is not practically valid because the monitoring statistic must remain nonnegative; hence, such values are set to zero.

Table 3
Components M_1 and M_2 for the MHWMA chart at $\rho = 0.1$.

Time index (k)	Sample size = 4		Sample size = 6		Sample size = 8	
	M_1	M_2	M_1	M_2	M_1	M_2
1	0.9934	1.0066	0.9945	1.0055	0.9953	1.0047
2	0.3442	1.6558	0.4602	1.5398	0.5359	1.4641
3	0.5363	1.4637	0.6183	1.3817	0.6718	1.3282
4	0.6214	1.3786	0.6883	1.3117	0.7320	1.2680
5	0.6721	1.3279	0.7301	1.2699	0.7679	1.2321
6	0.7067	1.2933	0.7585	1.2415	0.7924	1.2076
7	0.7322	1.2678	0.7796	1.2204	0.8105	1.1895
8	0.7521	1.2479	0.7959	1.2041	0.8245	1.1755
9	0.7681	1.2319	0.8091	1.1909	0.8359	1.1641
10	0.7813	1.2187	0.8200	1.1800	0.8452	1.1548
11	0.7925	1.2075	0.8292	1.1708	0.8532	1.1468
12	0.8022	1.1978	0.8372	1.1628	0.8600	1.1400

4. Performance evaluation

We present the features of the RL distribution of the proposed control chart in this section. These characteristics are used to assess the statistical efficacy of the proposed MHMWA chart. Furthermore, a comprehensive simulation is performed to evaluate the performance of the MHWMA chart. Even when a manufacturing process is IC, the proposed chart may falsely signal that the process is OC. This phenomenon occurs because the control limits act as decision thresholds, and the data being observed are inherently random. Specifically, this scenario is referred to as a Type-I error in hypothesis testing. In terms of hypothesis testing, this problem can be formulated as follows:

$$H_0 : \beta^2 = \beta_0^2 \quad \text{i.e., the Maxwell process is stable at } \beta_0$$

$$H_1 : \beta^2 = \beta_1^2 = \delta\beta_0^2 \quad \text{i.e., the process is shifted to scale parameter } \beta_1$$

where $\delta \geq 1$ denotes the shift constant domain since an increase in variability is considered more critical in the Maxwell monitoring scheme.

The RL consists of samples taken from the start of the observation period until the process triggers an OC signal. The RL is a random variable since it is established by observing samples that are considered independent and uniformly distributed. The average of RL is a key metric for control charts for both IC (ARL_0) and OC (ARL_1) states. Ideally, an effective control chart would have a low ARL_1 (i.e., quickly signaling true OC states) and a high ARL_0 (i.e., avoiding false alarms). However, achieving both optimal conditions simultaneously is frequently challenging. To find a good balance, achieving a suitable compromise in control chart design often involves setting ARL_1 to a specific value and subsequently minimizing ARL_1. Due to the high skewness and substantial variation often found in Maxwell data, the use of the ARL as a performance metric might not be appropriate. In addition, we also considered the MRL and standard deviation RL (SDRL) as measures of performance. Given the values of n, δ and β, the algorithm outlined in the following pseudocode allows us to determine the chart-estimated RL distribution and its key metrics. Let K be the number of replicated simulations. We set $K = 10000$ in this case, and for each ith run, we calculated RL_i as follows:

Step 1: Independently generate a random sample of a specific size from the Maxwell model, characterized by its scale parameter β.

Step 2: Initialize the process by setting $Q_0 = \beta_0^2$ at $i = 1$.

Step 3: Use Eq. (11) to compute the recursive statistic H_k, and subsequently the plotting statistic P_k using Eq. (12).

Step 4: If $P_j >$ UCL or $P_j <$ LCL, record RL=i and stop the loop; otherwise, proceed to the next loop i=i+1.

Step 5: Repeat these steps K times to obtain K RL values.

After replication, the ARL, MRL and SD values can be estimated by calculating the mean, median, and standard deviation of the run length values $\{RL(i)\}_{i=1}^{K}$.

We evaluated the performance of the proposed MHWMA control chart in terms of monitoring Maxwell-distributed processes across various settings of the smoothing parameter ρ. Tables 4–6 provide a summary of these findings for $\rho = 0.03$, $\rho = 0.25$ and $\rho = 0.75$, respectively. For each scenario, the ARL, MRL and SD are reported across a range of shift magnitudes (δ) from 1 to 3. Furthermore, the results are provided for three subgroup sizes $n = 3$, $n = 5$ and $n = 10$.

The data in Table 4 indicate that the MHWMA chart is acceptably sensitive to process changes. The ARL, MRL, and SDRL values decrease as the shift magnitude increases. Overall, larger sample sizes consistently improve the detection performance, as evidenced by the reduced ARL, MRL, and SDRL values. Extending the analysis to a higher smoothing parameter, Tables 5–6 presents similar patterns. This finding indicates that the chart detects shifts more quickly as the process deviation increases. A comparison of the data in Table 4 and Tables 5–6 reveals that a higher result generally produces lower ARL, MRL, and SDRL values for most shifts, showing that a larger ρ makes the chart more responsive to recent process changes. The higher values of the smoothing constant δ provide a more balanced and practically stable monitoring performance, whereas lower values such as $\delta = 0.03$ behave as a highly memory-dependent chart with a more dispersed run length behavior. This behavior is typical for EWMA charts, where a

Table 4
Performance metrics of the proposed control chart for different sample sizes at a fixed smoothing parameter $\rho = 0.03$.

Shifting parameter (δ)	$\rho = 0.03$								
	$n = 3$			$n = 5$			$n = 10$		
	ARL	MRL	SDRL	ARL	MRL	SDRL	ARL	MRL	SDRL
1.00	370.35	37	747.51	370.05	37	747.77	370.25	9	669.09
1.05	173.65	60	259.10	111.48	46	152.40	60.83	28	79.70
1.09	65.07	30	86.43	42.53	22	53.39	23.82	14	26.58
1.15	28.59	16	33.93	18.26	11	20.21	10.89	7	10.72
1.20	18.58	11	20.47	12.38	8	12.55	7.30	6	6.34
1.25	12.99	8	13.32	9.00	6	8.44	5.54	4	4.55
1.50	5.13	4	4.44	3.74	3	2.95	2.47	3	1.69
1.75	3.37	3	2.64	2.48	1	1.78	1.66	1	1.10
2.00	2.58	3	1.91	1.89	1	1.32	1.31	1	0.77
3.00	1.49	1	0.98	1.18	1	0.60	1.02	1	0.18

Table 5
Performance metrics of the MHWMA control chart for different sample sizes at a fixed smoothing parameter $\rho = 0.25$.

Shifting parameter (δ)	$\rho = 0.25$								
	$n = 3$			$n = 5$			$n = 10$		
	ARL	MRL	SDRL	ARL	MRL	SDRL	ARL	MRL	SDRL
1.00	370.07	308	282.38	369.96	308	289.60	370.00	317	285.20
1.05	170.18	148	124.01	119.01	101	89.88	85.30	73	63.50
1.09	107.77	94	77.35	62.71	54	46.87	40.37	35	30.79
1.15	62.74	55	45.98	32.25	28	24.30	18.87	16	13.93
1.20	43.39	38	32.39	21.44	19	16.02	12.07	10	8.76
1.25	33.01	29	24.53	14.93	13	11.42	8.58	7	5.99
1.50	11.89	9	9.44	5.41	5	3.92	3.33	3	2.12
1.75	6.62	5	5.11	3.27	3	2.18	2.08	1	1.31
2.00	4.67	4	3.51	2.42	2	1.58	1.54	1	0.94
3.00	2.30	1	1.55	1.31	1	0.73	1.04	1	0.26

Table 6
Performance metrics of the MHWMA control chart for different sample sizes at a fixed smoothing parameter $\rho = 0.75$.

Shifting parameter (δ)	$\rho = 0.75$								
	$n = 3$			$n = 5$			$n = 10$		
	ARL	MRL	SDRL	ARL	MRL	SDRL	ARL	MRL	SDRL
1.00	370.08	253.0	375.15	369.95	256.0	361.80	369.91	256	372.72
1.05	234.49	165.0	233.32	193.88	138.0	190.96	148.32	103	145.09
1.09	167.74	121.5	159.55	117.27	82.0	112.97	78.84	56	76.83
1.15	105.63	75.0	102.25	63.35	45.5	59.64	36.01	26	33.20
1.20	75.76	54.0	72.98	41.30	30.0	38.84	21.55	16	19.59
1.25	58.14	41.0	54.45	28.08	21.0	25.70	14.34	10	12.95
1.50	19.33	14.0	17.49	7.97	6.0	6.56	4.06	3	2.98
1.75	9.72	7.0	8.47	4.06	3.0	3.12	2.19	2	1.34
2.00	6.25	5.0	5.21	2.69	2.0	1.85	1.58	1	0.80
3.00	2.52	2.0	1.74	1.36	1.0	0.64	1.05	1	0.23

higher ρ emphasizes recent data, leading to quicker detection of moderate to large shifts at the expense of a slightly reduced ARL_0. In general, the results from both tables consistently indicate that the proposed chart effectively detects process shifts in Maxwell processes across different shifts and subgroup sizes. The smoothing parameter can be tuned to achieve the desired balance between detection sensitivity and chart stability depending on the specific monitoring objectives. It is important to note that sensitivity to process shifts cannot be improved by simply narrowing the control limits, as this would inflate the Type-I error rate beyond the nominal level. Instead, sensitivity gains are achieved by appropriately tuning the design parameters, namely, the smoothing constant ρ and the subgroup size n, while L is recalibrated via simulation (see Appendix) to maintain the target ARL_0.

5. Power comparisons

The performance of the proposed MHWMA chart was also evaluated relative to that of existing competitors, i.e., the V chart and the VEWMA chart, in terms of their power values for various shift magnitudes. Within the control chart framework, this comparison reveals the likelihood of correctly identifying a substandard quality batch and allowing a well-performing process to continue with regard to a particular quality characteristic. Control charts are designed to determine when the underlying distribution of a process

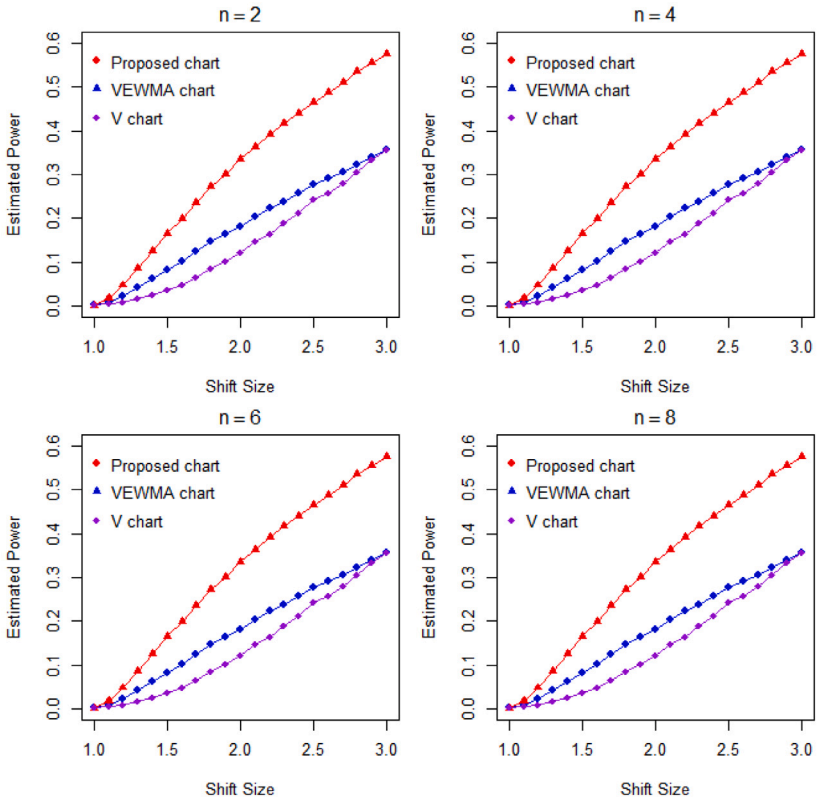


Fig. 2. Power comparisons of the proposed chart with the existing designs.

has changed. It is thus important to link process monitoring to the hypothesis testing framework discussed in Section 4. Specifically, *power* signifies the probability of accurately identifying an OC process when it has, in fact, shifted to the OC state. To evaluate the performance of the proposed chart in comparison to its competitors, the V and VEWMA charts, the power is defined as follows:

$$\begin{aligned}\text{Power} &= \Pr(\text{Reject } H_0 \mid H_0 \text{ is false}) \\ &= \Pr(\text{Signal} \mid \text{Process is in OC state})\end{aligned} \tag{27}$$

The power of a chart reflects its ability to detect process changes: a higher value means that it is better at detecting OC conditions. To conduct this comparison, we adjusted the shift amount from 1.0 to 3.0, increasing it by 0.1 each time. We then performed the analysis by using a fixed smoothing constant value of $\rho = 0.1$ for the proposed and VEWMA charts with a corresponding $ARL_0 = 370$. We also assumed that our Maxwell process is stable, with a scale value equal to 1.5. Based on our simulation outcomes, we determined the estimated power of the MHWMA and VEWMA charts for each setup. Fig. 2 illustrates the power profiles of the proposed MHWMA chart compared with those of the VEWMA chart across various smoothing constant values.

The comparison in Fig. 2 not only includes the estimated power of the V chart, VEWMA chart, and the proposed chart but also evaluates different sample sizes ($n = 2, 4, 6, 8$) across a range of shift values. It shows that the power of all three charts increases consistently with the magnitude of the change, which is consistent with the theoretical expectations. However, for various shift sizes, the power performance of the proposed chart is superior to that of the existing charts. The VEWMA chart performs moderately, generally better than the V chart but slightly below the proposed chart, while the V chart has the lowest power, particularly for small sample sizes and small shifts. For $n = 2$, all of the charts exhibit low power for small shifts, but the proposed chart still leads, reaching approximately 0.57 for larger shifts compared with approximately 0.36 for both the VEWMA and V charts. As the sample size increases, the power of all of the charts improves, with the proposed chart benefiting the most, especially for moderate shifts. At $n = 6$, the proposed chart reaches a power of approximately 0.92 at the largest shift, while the VEWMA and V charts reach approximately 0.60 and 0.79, respectively. For $n = 8$, the proposed chart approaches near-perfect detection with a power exceeding 0.96, whereas the VEWMA and V charts achieve approximately 0.68 and 0.89, respectively. Overall, the data in Fig. 2 illustrate that the proposed chart is the most effective for detecting both small and large shifts, the VEWMA chart offers moderate performance, and the V chart, although it improves with larger sample sizes, remains the least sensitive. This visual comparison emphasizes the advantages of the proposed chart for early and reliable process monitoring.

6. Steady-state performance evaluation

While the HWMA scheme has faced valid criticism for potential inertia effects in steady-state performance when process shifts occur after prolonged in-control periods [76–79], a thorough evaluation of the proposed MHWMA chart under realistic steady-state conditions is essential. To provide a more realistic assessment of detection performance, this section presents a comparative analysis of the proposed MHWMA chart and the existing VEWMA chart under steady-state conditions. In control chart theory, the performance of a control chart is traditionally evaluated using the zero-state ARL. Zero-state ARL assumes that the process shift occurs simultaneously with the start of monitoring ($t = 1$). In practice, this is often an unrealistic assumption, as shifts typically may occur at a random point in time ($t > 1$) after the process has been running in an in-control state for some duration. As noted by Knoth et al. [77], focusing solely on zero-state metrics can be misleading, particularly for memory-based charts. Some charts may exhibit rapid detection at the startup but suffer from poor weighting schemes that delay detection when a shift occurs later. Therefore, to evaluate the proposed control chart for the Maxwell scale parameter realistically, we utilize the conditional expected delay (CED). Let L be the run length stopping time, representing the number of observations until an alarm is flagged. If a process shift in the Maxwell scale parameter occurs at time t, the CED is defined as the expected delay in detection, given that no false alarm occurred before the shift. Following the work of Knoth et al. [76], the CED at change-point t is expressed as:

$$D_t = E_t(L - t + 1 \mid L \geq t) \tag{28}$$

where t is the time at which the shift in the Maxwell scale parameter occurs and the condition $L \geq t$ ensures that the chart has not produced a false alarm prior to the shift. As the time t increases, the CED typically converges to a limiting value, known as the conditional steady-state ARL. For the proposed Maxwell scale parameter chart, the steady-state ARL provides a more robust measure of performance than the zero-state ARL. It ensures that the weighting of past observations does not adversely affect the chart's ability to detect a change in the scale parameter once the process has reached a stable operating state. In our study, we evaluate the CED metric across various shift sizes (δ) and change-points (t). This allows us to ensure that the proposed chart maintains high sensitivity to shifts in the Maxwell scale parameter regardless of when the shift occurs. To address the performance of proposed chart, the CED was evaluated for different values of smoothing parameter and shift constant. In the computational setup we examined multiple delay values (t) ranging from 1 to 800 at various shifts (δ) in the process parameter. In this context, t refers to the number of IC samples before a change occurs in the scale parameter of Maxwell quality characteristic with $t = 1$ indicating a zero-state shift. For a fair comparison, both the MHWMA and VEWMA control charts are analyzed using identical values of the smoothing parameter ρ, $ARL_0 = 370$ and $n = 4$. Specifically, ρ weight is given to the present sample, and the remaining weight, $1 - \rho$, is distributed across all previous observations. However, MHWMA and VEWMA charts differ in the way that the remaining $1 - \rho$ is allocated to past samples. A Monte Carlo simulation study was conducted for comparative analysis, and the CED profiles are presented in Figs. 3–4 using 10^4 replications.

Fig. 3 illustrates the CED profiles of the proposed MHWMA chart and the VEWMA chart for different shift magnitudes ($\delta = 1.25,\ 2,\ 3,\ 4$) when the smoothing parameter is set to $\rho = 0.03$. It is observed that the CED of the proposed MHWMA chart increases monotonically as the change-point t increases for all shift sizes. This indicates that the MHWMA control chart takes some to reach the steady state . In contrast, the VEWMA chart exhibits relatively stable CED values across all values of t, suggesting consistent steady-state performance. For small shifts ($\delta = 1.25$), the difference between the two charts is particularly pronounced, with VEWMA maintaining significantly lower CED values. A similar pattern is observed for moderate and large shifts ($\delta = 2,\ 3,\ 4$), where the VEWMA chart outperforms the proposed chart in terms of steady-state detection delay, consistent with critiques of homogeneous weighting for small smoothing parameters. These results suggest that, for very small smoothing parameters, the proposed MHWMA chart is more sensitive to initial observations but suffers from reduced responsiveness when the process shift occurs after a prolonged in-control period. In addition, Fig. 4 presents the CED profiles for both charts when the smoothing parameter is increased to $\rho = 0.25$. In this case, the behavior of the proposed MHWMA chart changes notably. For small shifts ($\delta = 1.25$), the VEWMA chart continues to exhibit lower and more stable CED values, indicating better performance. However, for moderate and large shifts ($\delta = 2,\ 3,\ 4$), the proposed chart demonstrates a different trend. Specifically, the CED of the MHWMA chart initially increases for small values of t, but then decreases and stabilizes as t grows. For larger shift magnitudes ($\delta = 3$ and $\delta = 4$), the proposed chart eventually achieves lower steady-state CED values than the VEWMA chart, indicating improved detection capability when the process shift occurs after a sufficiently long in-control period. This behavior suggests that increasing the smoothing parameter mitigates the inertia effect and allows the proposed chart to respond more effectively to recent observations. We can infer that HWMA-type charts in case of Maxwell distribution can exhibit superiority regions under suitable parameters. Moreover, by expanding the statistic of the proposed chart, given in Eq. (12), it becomes evident that the proposed scheme follows a rational weighting pattern, assigning progressively smaller weights to past observations relative to current data. As a result, the MHWMA chart exhibits superior steady-state performance in detecting moderate-to-large shifts under appropriate parameter settings. We observed a similar pattern for different values of sample and the smoothing parameter; however, the corresponding results are not reported here due to the consistent behavior across all settings. In general, the simulation results suggest that the VEWMA control chart exhibits superior steady-state performance for the Maxwell process under specific choices of design parameters. However, the VEWMA chart does not demonstrate uniform superiority instead both charts exhibit their own regions of superiority.

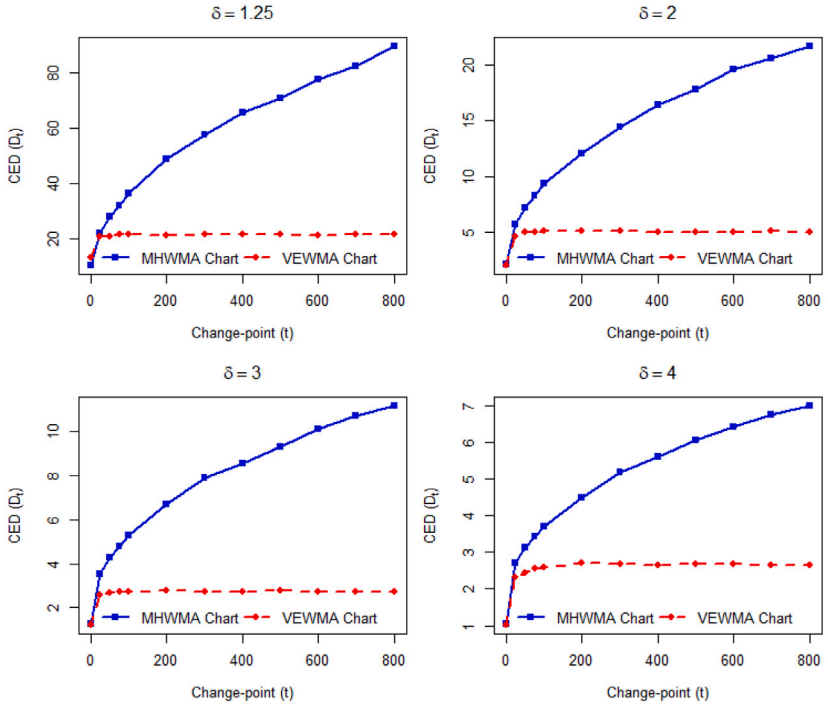


Fig. 3. Steady-state performance comparison of the MHWMA and VEWMA charts at $\rho = 0.03$.

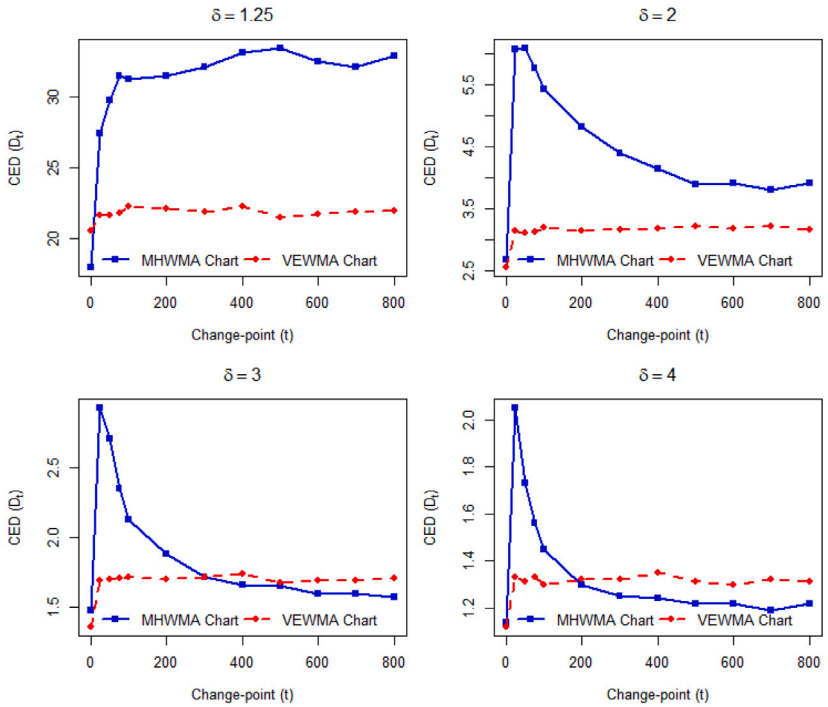


Fig. 4. Steady-state performance comparison of the MHWMA and VEWMA charts at $\rho = 0.25$.

Table 7
Data groups and plotting statistics computation.

1st	2nd	3rd	4th	T_i	P_k
0.309	2.229	4.570	2.964	2.895	2.595497
4.485	2.154	2.890	2.625	3.333	2.898896
1.652	2.089	3.117	2.038	1.747	3.100155
3.699	0.557	3.467	2.481	2.681	2.658390
2.661	1.248	3.114	2.135	1.908	2.656237
1.432	1.981	1.281	2.190	1.034	2.497816
1.281	1.619	3.103	1.615	1.375	2.257308
2.010	3.443	2.223	1.506	1.925	2.136756
4.602	2.962	1.505	3.924	3.968	2.130755
2.610	2.324	4.305	3.166	3.397	2.329177
3.779	4.449	4.376	1.911	4.740	2.449428
3.376	2.097	1.124	2.224	1.834	2.628570
3.578	1.568	2.085	0.943	1.708	2.561074
4.035	2.646	2.934	1.303	2.799	2.506370
4.255	1.866	1.757	2.385	2.530	2.524588
3.344	0.040	1.652	1.899	1.460	2.514259
1.070	3.000	1.480	4.278	2.553	2.459295
2.300	3.595	0.301	1.914	1.831	2.457586
4.167	3.478	2.632	4.121	4.448	2.448926
1.876	2.688	2.902	4.663	3.409	2.543732
2.194	2.823	4.240	1.912	2.868	2.581592

7. Real-data application study

In this section, the methodology of the proposed MHWMA chart is verified by using a real dataset from the aerospace industry. The dataset pertains to aircraft windshield failure cases and was initially utilized in warranty cost estimation and reliability analysis, with detailed information available in Murthy et al. [80]. The dataset has been previously used in SPC-related applications, as reported by Khan et al. [11]. In large aircraft, the windshield is a vital component that is constructed from multiple laminated material layers under high temperature and pressure. During flight, notably at take-off and landing, windshields are subjected to severe stress conditions. Typical failures are observed in the form of cracks in the outer layer, breakdown of the heating mechanism, or progressive degradation of the material, which eventually require replacement. Furthermore, maintaining optimal pilot visibility is critical for aircraft safety [81], and thus, different approaches have been implemented by manufacturers and operators to ensure clear vision through transparent surfaces. As a result, aerospace glass manufacturers routinely collect and evaluate windshield data to optimize design and quality standards with the aim of consistent performance under varying flight conditions. The dataset comprises 84 measurements that correspond to windshield failure times and has also been utilized in several earlier studies in the context of applications of newly developed distributions [82–85]. To demonstrate the applicability of the proposed scheme, the dataset is organized into 21 subgroups, each containing 4 observations, as shown in Table 7.

Before we utilized the subgroups provided in Table 7 to construct the MHWMA chart, we assessed the adequacy of the Maxwell distribution for the windshield failures data. The MD properly fits the given dataset and has already been established in the work Khan et al. [11]. To confirm more rigorously whether the windshield failures data follow a MD, we employed visual diagnostics via PP and CDF plots as well as statistical verification with the Kolmogorov–Smirnov (KS) test. These methods provide a sufficient evaluation: the fitting plots reveal visual evidence of the correspondence between the given data and the theoretical model, whereas the KS test offers a quantitative indicator of fit. The fitting curves of the PP and CDF plots are shown in Fig. 5.

The PP plot illustrates the comparison between the theoretical probabilities predicted by the fitted Maxwell distribution and the empirical probabilities from the ordered values of the dataset. As shown in Fig. 5(a), the empirical quantiles match the theoretical values, indicating a good fit. Most of the data lie close to or along the reference line, suggesting that high agreement is observed, especially in the middle range where most of the data lies. The PP plot visually confirms that the Maxwell distribution captures the probabilistic structure of the data well. On the other hand, Fig. 5(b) also indicates that the empirical CDF of the data closely follows the theoretical CDF curve of the Maxwell distribution across the entire range, with only slight divergence at the lower tail. Thus, the visual diagnostics (i.e., the PP and CDF plots) provide qualitative assurance through visual alignment with no major systematic deviations. This confirmation allowed us to proceed with Maxwell-based inferences on the dataset with reasonable assurance. For further validation, we applied the KS test to quantitatively confirm the suitability of the Maxwell distribution for our data. As a nonparametric approach, the KS evaluates how well the empirical CDF of the data fits with the theoretical CDF of the fitted Maxwell distribution. The test calculates the maximum vertical deviation (D) between the two cumulative distribution functions under the null hypothesis that the data follow the Maxwell distribution. The results of the KS test yielded a D statistic equal to 0.066, with a p value of approximately 0.833 ; the small value of D and larger value of p suggest that the data are consistent with the Maxwell distribution. To illustrate the implementation procedure for the proposed chart, the last column reports the preliminary sample statistics, which were computed according to Eq. (12). From Table 1, an appropriate smoothing constant denoted by ρ can be

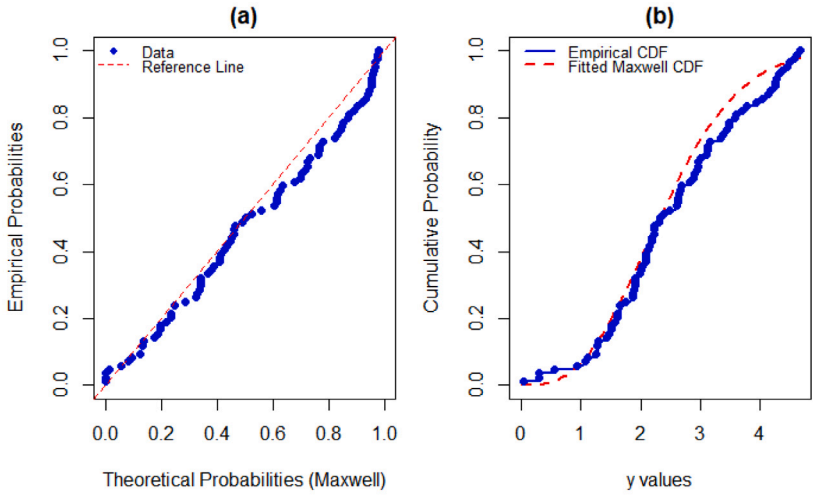


Fig. 5. Fitting plots depicting the windshield failures data: (a) PP plot and (b) CDF plot.

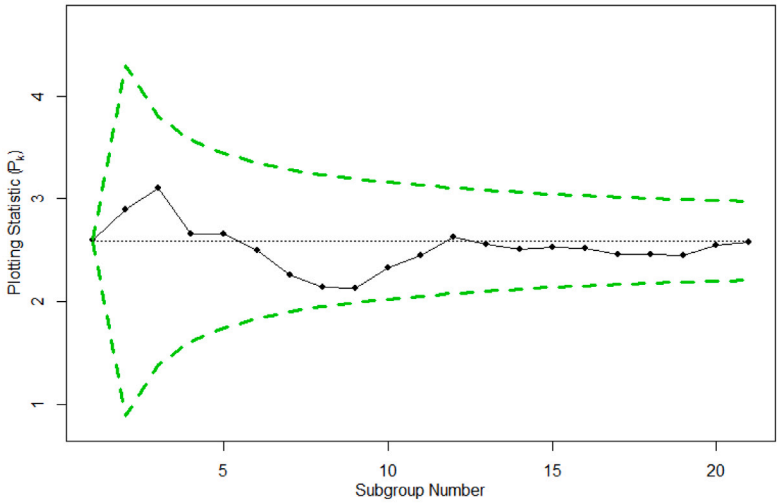


Fig. 6. MHWMA control chart for windshield failure measurements.

identified for a subgroup sample size of 4. By referring to this table, we selected the control chart coefficient $L = 1.6224$ for $n = 4$ at $\rho = 0.1$. Subsequently, the critical value L was employed to compute the values of $M_{1,k}$ and $M_{2,k}$, along with the lower and upper control limits (LCL and UCL) by using Eq. (26). For the given data, the penultimate column of Table 6 provides the estimated value of T_k by using Eq. (4), which provides the overall mean value $\hat{\beta^2} = 2.5925$. The plotting statistics based on the selected parameters were computed with Eq. (12) and are presented in the last column of Table 7. The parameters of the proposed chart are shown in Fig. 6 such that any departure from the mean value can be identified; the process is in the IC state at $CL = 2.5925$.

As shown in Fig. 6, the plotting statistic P_k remains within the specified control limits, confirming that no OC signals exist. To further assess the sensitivity of the MHWMA chart, we introduced an artificial shift in the monitoring statistics by inflating the IC of $\hat{\beta^2}$ by 10%. Specifically, we generated an additional 10 subgroup statistics from a Gamma distribution scaled by $\hat{\beta}_1^2 = 1.10 * \hat{\beta}^2$, representing an OC scenario. In this setup, the extended dataset was formed by combining the 21 Phase-1 subgroups followed by 10 subgroups representing the OC condition. The plotting statistics and corresponding control limits of the MHWMA control chart were recalculated by using the same parameters ($n = 4$, $\rho = 0.1$, and $L = 1.6624$), and the resulting chart for the given scenario is depicted in Fig. 7.

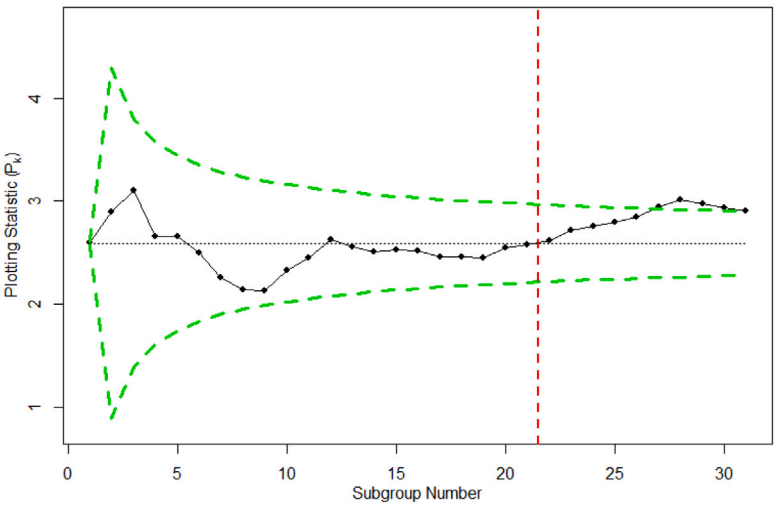


Fig. 7. MHWMA control chart for the windshield failure measurements, showing the transition from 21 IC subgroups to 10 OC subgroups.

Fig. 7 clearly indicates that the OC measurements exceed the control limits, thereby demonstrating that the proposed MHWMA chart is capable of detecting smaller and moderate process shifts efficiently.

8. Conclusions

In this article, we proposed and evaluated a new memory-type monitoring scheme specifically designed for the scale parameter of the Maxwell-distributed quality characteristics [C1]. The proposed scheme is known as the MHWMA control chart, and it assigns weights to the observations such that the recent sample receives a specific weight while the remaining weight is equally distributed among the previous samples. By incorporating a different weighting mechanism, the proposed control chart yields an improvement over the existing VEWMA control chart, which relies on the conventional EWMA weighting pattern. The underlying theoretical characteristics of the suggested scheme have been established, and the framework for its control limits has been determined. The RL performance measures of the MHWMA chart have been provided by means of Monte Carlo simulations, and the run-length performance demonstrated that the MHWMA chart provides a superior alternative to the existing monitoring schemes designed for Maxwell processes [C2]. A comparative analysis with the existing counterpart was also carried out, further confirming its superior performance in terms of both sensitivity and efficiency. Furthermore, the steady-state analysis reveals that the MHWMA chart is capable of maintaining its dominance over the VEWMA chart, even when the process shift occurs after a delay, provided suitable design parameters are selected. However, a notable limitation of the proposed MHWMA chart is its sensitivity to the smoothing parameter ρ, exhibiting some inertia effects and higher CED compared to the VEWMA chart in steady-state conditions when small values of ρ are used, particularly for small shifts. The application to real data from the aerospace industry validated the practical utility of the MHWMA chart in engineering contexts, where the Maxwell distribution better represents the underlying process [C3].

Although the proposed MHWMA chart demonstrates excellent performance in terms of detecting small shifts in Maxwell distributed processes, opportunities for improvement still exist. Specifically, developing a multivariate version of the MHWMA chart for complex engineering systems and exploring its behavior when the process deviates from the Maxwell assumption could provide valuable contributions in future work. In addition, future research could explore adaptive smoothing parameter or hybrid schemes to further optimize steady-state performance across all shift sizes.

Declaration of competing interest

The authors declare that they have no known competing financial interests or personal relationships that could have appeared to influence the work reported in this paper.

Appendix

Algorithm 1 Simulation-based computation of the L factor

Input: Target ARL_0, β^2, n, ρ, search bounds $[\rho_L, \rho_U]$
Output: Estimated L and actual ARL_0
$K \leftarrow 10000$ ▷ Number of replications
$N \leftarrow 4000$ ▷ Maximum sequence length
while not converged **do**
  $\rho_t \leftarrow (\rho_L + \rho_U)/2$
  $AARL0 \leftarrow 0$
  for $j \leftarrow 1$ to K **do**
    $C \leftarrow$ A zero vector of size N
    $H \leftarrow$ A zero vector of size N ▷ MHWMA plotting statistic
    $X \leftarrow$ Generate N observations from $MD(\beta)$
    Initialize monitoring statistic $H[1] \leftarrow \rho^2 X_1 + (1-\rho^2)\beta^2$
    $C[1] \leftarrow L\beta^2\sqrt{\frac{2}{3n}\rho^4}$
    if $H[1]$ exceeds limits **then**
      Record run length = 1; **continue**
    end if
    for $i \leftarrow 2$ to N **do**
      $C[i] \leftarrow \rho\beta^2\sqrt{\frac{2}{3n}\left(\rho^4 + \frac{(1-\rho^2)^2}{i-1}\right)}$
      Update $H[i] \leftarrow \rho^2 X_i + (1-\rho^2)\overline{X}_{1:(i-1)}$
      if $H[i]$ exceeds limits **then**
        Record run length = i; **break**
      end if
    end for
  end for
  $AARL0 \leftarrow$ average of recorded run lengths
  if $AARL0 <$ Target **then**
    $\rho_L \leftarrow \rho_t$
  else
    $\rho_U \leftarrow \rho_t$
  end if
end while

Data availability

Data will be made available on request.

References

[1] Haridy S, Maged A, Alherimi N, Shamsuzzaman M, Al-Ali S. Optimization design of control charts: A systematic review. Qual Reliab Eng Int 2024;40(4):2122–57. http://dx.doi.org/10.1002/qre.3490.
[2] Jiang R, Yu Z, Zhang J, Sun F, Parmar M. Multiple 'memory-based'schemes for monitoring Maxwell distributions with measurement errors. J Stat Comput Simul 2025;1–42. http://dx.doi.org/10.1080/00949655.2025.2450076.
[3] Qiu P. Introduction to statistical process control. CRC Press; 2013.
[4] Bisiotis K, Psarakis S, Yannacopoulos AN. Control charts in financial applications: An overview. Qual Reliab Eng Int 2022;38(3):1441–62. http://dx.doi.org/10.1002/qre.2962.
[5] Hajej Z, Nyoungue AC, Abubakar AS, Mohamed Ali K. An integrated model of production, maintenance, and quality control with statistical process control chart of a supply chain. Appl Sci 2021;11(9):4192. http://dx.doi.org/10.3390/app11094192.
[6] Montgomery DC. The 100th anniversary of the control chart. J Qual Technol 2024;56(1):2–4. http://dx.doi.org/10.1080/00224065.2023.2282926.
[7] Gunay E, Kula U. Integration of production quantity and control chart design in automotive manufacturing. Comput Ind Eng 2016;102:374–82. http://dx.doi.org/10.1016/j.cie.2016.06.016.
[8] Aykroyd RG, Leiva V, Ruggeri F. Recent developments of control charts, identification of big data sources and future trends of current research. Technol Forecast Soc Change 2019;144:221–32. http://dx.doi.org/10.1016/j.techfore.2019.01.005.
[9] Fu X, Wang Rf, Dong Zy. Application of a shewhart control chart to monitor clean ash during coal preparation. Int J Miner Process 2017;158:45–54. http://dx.doi.org/10.1016/j.minpro.2016.11.019.
[10] Khan Z, Shah F, Katona AI, Kosztyán ZT. Enhanced process monitoring for the Maxwell process via the cUSum control chart and its application to the carbon fiber industry. IEEE Access 2024. http://dx.doi.org/10.1109/ACCESS.2024.3494042.

[11] Khan Z, Saghir A, Katona A, Kosztyan ZT. EWMA control chart framework for efficient Maxwell quality characteristic monitoring: An application to the aerospace industry. Comput Ind Eng 2025;200:110753. http://dx.doi.org/10.1016/j.cie.2024.110753.

[12] Vera do Carmo C, Lopes LFD, Souza AM. Comparative study of the performance of the CuSum and EWMA control charts. Comput Ind Eng 2004;46(4):707–24. http://dx.doi.org/10.1016/j.cie.2004.05.025.

[13] Lucas JM. Combined shewhart-CUSUM quality control schemes. J Qual Technol 1982;14(2):51–9. http://dx.doi.org/10.1080/00224065.1982.11978790.

[14] Lucas JM, Saccucci MS. Exponentially weighted moving average control schemes: properties and enhancements. Technometrics 1990;32(1):1–12. http://dx.doi.org/10.1080/00401706.1990.10484583.

[15] Zaman B, Riaz M, Abbas N, Does RJ. Mixed cumulative sum–exponentially weighted moving average control charts: an efficient way of monitoring process location. Qual Reliab Eng Int 2015;31(8):1407–21. http://dx.doi.org/10.1002/qre.1678.

[16] Abbas N, Riaz M, Does RJ. Mixed exponentially weighted moving average–cumulative sum charts for process monitoring. Qual Reliab Eng Int 2013;29(3):345–56. http://dx.doi.org/10.1002/qre.1385.

[17] Sheu SH, Lin TC. The generally weighted moving average control chart for detecting small shifts in the process mean. Qual Eng 2003;16(2):209–31. http://dx.doi.org/10.1081/QEN-120024009.

[18] Ali R, Haq A. A mixed GWMA–CUSUM control chart for monitoring the process mean. Comm Statist Theory Methods 2018;47(15):3779–801. http://dx.doi.org/10.1080/03610926.2017.1361994.

[19] Taboran R, Sukparungsee S, Areepong Y. Mixed moving average-exponentially weighted moving average control charts for monitoring of parameter change. In: Proceeding of the international multiConference of engineers and computer scientists. 2019, p. 13–5.

[20] Talordphop K, Sukparungsee S, Areepong Y. New modified exponentially weighted moving average-moving average control chart for process monitoring. Connect Sci 2022;34(1):1981–98. http://dx.doi.org/10.1080/09540091.2022.2090513.

[21] Abbas N. Homogeneously weighted moving average control chart with an application in substrate manufacturing process. Comput Ind Eng 2018;120:460–70. http://dx.doi.org/10.1016/j.cie.2018.05.009.

[22] Abid M, Mei S, Nazir HZ, Riaz M, Hussain S. A mixed HWMA-CUSUM mean chart with an application to manufacturing process. Qual Reliab Eng Int 2021;37(2):618–31. http://dx.doi.org/10.1002/qre.2752.

[23] Abid M, Mei S, Nazir HZ, Riaz M, Hussain S, Abbas Z. A mixed cumulative sum homogeneously weighted moving average control chart for monitoring process mean. Qual Reliab Eng Int 2021;37(5):1758–71. http://dx.doi.org/10.1002/qre.2824.

[24] Zaman B, Riaz M, Lee MH. On the performance of control charts for simultaneous monitoring of location and dispersion parameters. Qual Reliab Eng Int 2017;33(1):37–56. http://dx.doi.org/10.1002/qre.1989.

[25] ur Rehman A, Shabbir J, Munir T, Ahmad S, Riaz M. Ameliorating the diagnostic power of combined shewhart-memory-type control chart strategies for mean. J Stat Comput Simul 2024;94(11):2564–95. http://dx.doi.org/10.1080/00949655.2024.2346136.

[26] Talordphop K, Areepong Y, Suparungsee S. An enhanced mixed moving average—Homogeneously weighted moving average control chart to monitor the mean process. Lobachevskii J Math 2024;45(9):4378–86. http://dx.doi.org/10.1134/S1995080224605010.

[27] Teoh WL, Yeong WC, Khoo MB, Teh SY. The performance of the double sampling X chart with estimated parameters for skewed distributions. Acad J Sci 2016;5(1):237–52.

[28] Tuh M, Lee M, Lau E, Then PH. Performance of the double sampling np chart based on the median run length. Adv Math: Sci J 2020;9(9):7429–38. http://dx.doi.org/10.37418/amsj.9.9.89.

[29] Tuh MH, Kon CML, Chua HS, Lau MF. Optimal statistical design of the double sampling np chart based on expected median run length. Front Appl Math Stat 2022;8:993152. http://dx.doi.org/10.3389/fams.2022.993152.

[30] Tuh MH, Kon CML, Chua HS, Lau MF, Chang YHR. Evaluating the performance of synthetic double sampling np chart based on expected median run length. Mathematics 2023;11(3):595. http://dx.doi.org/10.3390/math11030595.

[31] Borror CM, Montgomery DC, Runger GC. Robustness of the EWMA control chart to non-normality. J Qual Technol 1999;31(3):309–16. http://dx.doi.org/10.1080/00224065.1999.11979929.

[32] Noiplab T, Mayureesawan T. Modified EWMA control chart for skewed distributions and contaminated processes. Thail Stat 2019;17(1):16–29.

[33] Noorossana R, Fathizadan S, Nayebpour MR. EWMA control chart performance with estimated parameters under non-normality. Qual Reliab Eng Int 2016;32(5):1637–54. http://dx.doi.org/10.1002/qre.1896.

[34] Huwang L, Lin LW. New EWMA control charts for monitoring the Weibull shape parameter. Qual Reliab Eng Int 2020;36(6):1872–94. http://dx.doi.org/10.1002/qre.2663.

[35] Alduais FS, Khan Z. EWMA control chart for Rayleigh process with engineering applications. IEEE Access 2023;11:10196–206.

[36] Sanaullah A, Chaudhary AM, Hanif M, Sharma P. EWMA control charts based on robust estimators: A powerful tool for monitoring a process with a non-normal distribution. J Comput Appl Math 2024;449:115919. http://dx.doi.org/10.1016/j.cam.2024.115919.

[37] Human SW, Kritzinger P, Chakraborti S. Robustness of the EWMA control chart for individual observations. J Appl Stat 2011;38(10):2071–87. http://dx.doi.org/10.1080/02664763.2010.545114.

[38] Liu JY, Xie M, Goh TN, Chan L. A study of EWMA chart with transformed exponential data. Int J Prod Res 2007;45(3):743–63. http://dx.doi.org/10.1080/00207540600792598.

[39] Abbasi SA, Riaz M, Miller A, Ahmad S, Nazir HZ. EWMA dispersion control charts for normal and non-normal processes. Qual Reliab Eng Int 2015;31(8):1691–704. http://dx.doi.org/10.1002/qre.1702.

[40] Saghir A, Ahmad L, Aslam M. Modified EWMA control chart for transformed gamma data. Comm Statist Simulation Comput 2021;50(10):3046–59. http://dx.doi.org/10.1080/03610918.2019.1619762.

[41] Gan F. Monitoring observations generated from a binomial distribution using modified exponentially weighted moving average control chart. J Stat Comput Simul 1990;37(1–2):45–60. http://dx.doi.org/10.1080/00949659008811293.

[42] Urbieta P, Lee HO L, Alencar A. CUSUM and EWMA control charts for negative binomial distribution. Qual Reliab Eng Int 2017;33(4):793–801. http://dx.doi.org/10.1002/qre.2057.

[43] Ryan AG, Woodall WH. Control charts for Poisson count data with varying sample sizes. J Qual Technol 2010;42(3):260–75. http://dx.doi.org/10.1080/00224065.2010.11917823.

[44] Zaka A, Akhter AS, Jabeen R, Sanaullah A. Control charts for the shape parameter of reflected power function distribution under classical estimators. Qual Reliab Eng Int 2021;37(6):2458–77. http://dx.doi.org/10.1002/qre.2866.

[45] Jabeen R, Zaka A. The modified control charts for monitoring the shape parameter of weighted power function distribution under classical estimator. Qual Reliab Eng Int 2021;37(8):3417–30. http://dx.doi.org/10.1002/qre.2925.

[46] Calzada ME, Scariano SM. The robustness of the MaxEWMA chart to non-normality. Comm Statist Simulation Comput 2003;32(2):573–90. http://dx.doi.org/10.1081/SAC-120017507.

[47] Alkahtani SS. Robustness of DEWMA versus EWMA control charts to non-normal processes. J Mod Appl Stat Methods 2013;12(1):18. http://dx.doi.org/10.22237/jmasm/1367381820.

[48] Lin YC, Chou CY, Chen CH. Robustness of the EWMA median control chart to non-normality. Int J Ind Syst Eng 2017;25(1):35–58. http://dx.doi.org/10.1504/IJISE.2017.080687.

[49] Saeed N, Kamal S. New EWMA control charts for monitoring mean under non-normal processes using repetitive sampling. Iran J Sci Technol Trans A: Sci 2019;43:1215–25. http://dx.doi.org/10.1007/s40995-018-0586-9.
[50] Saeed N, Abu-Shawiesh MOA. A trimmed EWMA control charts for non-normal processes. Prod Eng 2021;15(3):545–61. http://dx.doi.org/10.1007/s11740-021-01039-1.
[51] Nazir HZ, Hussain T, Abbas Z, Akhtar N, Abid M, Riaz M. On developing robust adaptive approaches for monitoring location of non-normal environments. Qual Reliab Eng Int 2022;38(1):326–42. http://dx.doi.org/10.1002/qre.2979.
[52] Li D, Miao S. Fitting the wind speed probability distribution with Maxwell and power Maxwell distributions: A case study of North Dakota sites. Sustain Energy Technol Assess 2021;47:101446. http://dx.doi.org/10.1016/j.seta.2021.101446.
[53] Bekker A, Roux J. Reliability characteristics of the maxwell distribution: A Bayes estimation study. Comm Statist Theory Methods 2005;34(11):2169–78. http://dx.doi.org/10.1080/STA-200066424.
[54] Krishna H, Malik M. Reliability estimation in Maxwell distribution with type-II censored data. Int J Qual Reliab Manag 2009;26(2):184–95. http://dx.doi.org/10.1108/02656710910928815.
[55] Krishna H, Vivekanand, Kumar K. Estimation in Maxwell distribution with randomly censored data. J Stat Comput Simul 2015;85(17):3560–78. http://dx.doi.org/10.1080/00949655.2014.986483.
[56] Sharma VK, Bakouch HS, Suthar K. An extended maxwell distribution: Properties and applications. Comm Statist Simulation Comput 2017;46(9):6982–7007. http://dx.doi.org/10.1080/03610918.2016.1222422.
[57] Hernandez H. Standard Maxwell-Boltzmann distribution: definition and properties. ForsChem Res Rep 2017;2:1–16.
[58] Godase DG, Mahadik SB, Rakitzis AC. The SPRT control charts for the Maxwell distribution. Qual Reliab Eng Int 2022;38(4):1713–28. http://dx.doi.org/10.1002/qre.3047.
[59] Shah F, Aslam M, Khan Z. New control chart based on neutrosophic Maxwell distribution with decision making applications. Neutrosophic Sets Syst 2023;53:297–316.
[60] Arafat SY, Hossain MP, Ajadi JO, Riaz M. On the development of EWMA control chart for inverse Maxwell distribution. J Test Eval 2021;49(2):1086–103. http://dx.doi.org/10.1520/JTE20190082.
[61] Saghir A, Hu X, Tran KP, Song Z. Optimal design and evaluation of adaptive EWMA monitoring schemes for inverse Maxwell distribution. Comput Ind Eng 2023;181:109290. http://dx.doi.org/10.1016/j.cie.2023.109290.
[62] Waqas M, Xu SH, Anwar SM, Rasheed Z, Khan M. Enhanced adaptive EWMA control chart to observe inverse maxwell process with engineering and healthcare sector applications. Qual Reliab Eng Int 2025. http://dx.doi.org/10.1002/qre.3772.
[63] Shah F, Khan Z, Aslam M, Kadry S. Statistical development of the VSQ-control chart for extreme data with an application to the carbon fiber industry. Math Probl Eng 2021;2021(1):9766986. http://dx.doi.org/10.1155/2021/9766986.
[64] Hossain MP, Omar MH, Riaz M. New V control chart for the Maxwell distribution. J Stat Comput Simul 2017;87(3):594–606. http://dx.doi.org/10.1080/00949655.2016.1222391.
[65] Hossain MP, Sanusi RA, Omar MH, Riaz M. On designing Maxwell CUSUM control chart: an efficient way to monitor failure rates in boring processes. Int J Adv Manuf Technol 2019;100:1923–30. http://dx.doi.org/10.1007/s00170-018-2679-1.
[66] Hossain MP, Riaz M. On designing a new VEWMA control chart for efficient process monitoring. Comput Ind Eng 2021;162:107751. http://dx.doi.org/10.1016/j.cie.2021.107751.
[67] Aslam M, Khan M, Anwar SM, Zaman B. A homogeneously weighted moving average control chart for monitoring time between events. Qual Reliab Eng Int 2022;38(2):1013–44. http://dx.doi.org/10.1002/qre.3032.
[68] Anwar SM, Aslam M, Zaman B, Riaz M. An enhanced double homogeneously weighted moving average control chart to monitor process location with application in automobile field. Qual Reliab Eng Int 2022;38(1):174–94.
[69] Adegoke NA, Smith AN, Anderson MJ, Sanusi RA, Pawley MD. Efficient homogeneously weighted moving average chart for monitoring process mean using an auxiliary variable. IEEE Access 2019;7:94021–32. http://dx.doi.org/10.1109/ACCESS.2019.2926533.
[70] Adegoke NA, Abbasi SA, Smith AN, Anderson MJ, Pawley MD. A multivariate homogeneously weighted moving average control chart. IEEE Access 2019;7:9586–97. http://dx.doi.org/10.1109/ACCESS.2019.2891988.
[71] Alevizakos V, Chatterjee K, Koukouvinos C. The extended homogeneously weighted moving average control chart. Qual Reliab Eng Int 2021;37(5):2134–55. http://dx.doi.org/10.1002/qre.2849.
[72] Adeoti OA, Koleoso SO. A hybrid homogeneously weighted moving average control chart for process monitoring. Qual Reliab Eng Int 2020;36(6):2170–86. http://dx.doi.org/10.1002/qre.2690.
[73] Raza MA, Nawaz T, Han D. On designing distribution-free homogeneously weighted moving average control charts. J Test Eval 2020;48(4):3154–71. http://dx.doi.org/10.1520/JTE20180550.
[74] Abid M, Shabbir A, Nazir HZ, Sherwani RAK, Riaz M. A double homogeneously weighted moving average control chart for monitoring of the process mean. Qual Reliab Eng Int 2020;36(5):1513–27. http://dx.doi.org/10.1002/qre.2641.
[75] Montgomery DC. Introduction to statistical quality control. John wiley & sons; 2020.
[76] Knoth S, Tercero-Gómez VG, Khakifirooz M, Woodall WH. The impracticality of homogeneously weighted moving average and progressive mean control chart approaches. Qual Reliab Eng Int 2021;37(8):3779–94.
[77] Knoth S, Saleh NA, Mahmoud MA, Woodall WH, Tercero-Gómez VG. A critique of a variety of ‘‘memory-based" process monitoring methods. J Qual Technol 2023;55(1):18–42.
[78] Haq A, Woodall WH. A critique of the use of modified and moving average-based EWMA control charts. Qual Reliab Eng Int 2023;39(4):1269–76.
[79] Woodall WH, Saleh NA, Mahmoud MA, Tercero-Gómez VG, Knoth S. Misguided statistical process monitoring approaches. In: Advanced statistical methods in process monitoring, finance, and environmental science: essays in honour of wolfgang schmid. Springer; 2024, p. 211–20.
[80] Murthy DP, Xie M, Jiang R. Weibull models. John Wiley & Sons; 2004.
[81] Kwong E, Lee WB. Knowledge elicitation in reliability management in the airline industry. J Knowl Manag 2009;13(2):35–48. http://dx.doi.org/10.1108/13673270910942682.
[82] Tahir MH, Cordeiro GM, Mansoor M, Zubair M. The Weibull-Lomax distribution: properties and applications. Hacet J Math Stat 2015;44(2):455–74. http://dx.doi.org/10.15672/HJMS.2014147465.
[83] Elshahhat A, Abo-Kasem OE, Mohammed HS. Reliability analysis and applications of generalized type-II progressively hybrid Maxwell–Boltzmann censored data. Axioms 2023;12(7):618. http://dx.doi.org/10.3390/axioms12070618.
[84] Almazah MM, Alshahrani MA, Ramzan Q, Raza IA, Tahir M, Ahmad Z. Estimation of parameters for the modified Weibull distribution under step-stress accelerated life testing with application to aircraft windshields data: M. Almazah et al.. Sci Rep 2025;15(1):25137. http://dx.doi.org/10.1038/s41598-025-95469-x.
[85] Ashraf K, Akhtar N, Ramzan Q, Nazir HZ, Alballa T. Bayesian and classical insights into a novel probability model for aircraft windshield failures: Bayesian and classical insights into QR distribution. Qual Reliab Eng Int 2025. http://dx.doi.org/10.1002/qre.70028.